

# Physical Layer Security in Finite Blocklength Massive IoT with Randomly Located Eavesdroppers

Tijana Devaja\*, Milica Petkovic\*, Sokol Kosta<sup>†</sup>, Dejan Vukobratović\*, and Čedomir Stefanović<sup>†</sup>

\*Faculty of Technical Sciences, University of Novi Sad, Serbia ({tijana.devaja, milica.petkovic, dejanv}@uns.ac.rs)

<sup>†</sup>Department of Electronic Systems, Aalborg University, Aalborg, Denmark ({sok,cs}@es.aau.dk)

**Abstract**—This paper analyzes the physical layer security performance of massive uplink Internet of Things (IoT) networks operating under the finite blocklength (FBL) regime. IoT devices and base stations (BS) are modeled using a stochastic geometry approach, while an eavesdropper is placed at a random location around the transmitting device. This system model captures security risks common in dense IoT deployments. Analytical expressions for the secure success probability, secrecy outage probability and secrecy throughput are derived to characterize how stochastic interference, fading and eavesdropper spatial uncertainty interact with FBL constraints in short packet uplink transmissions. Numerical results illustrate key system behavior under different network and channel conditions.

**Index Terms**—Finite blocklength (FBL), massive Internet of Things (IoT), physical layer security (PLS), stochastic geometry.

## I. INTRODUCTION

Massive Internet of Things (IoT) networks are one of the key components of modern wireless communications, enabling large-scale connectivity among heterogeneous low-power devices [1]–[3]. In many practical scenarios, IoT nodes transmit short status updates or control packets, often under strict latency and reliability constraints. Such scenarios cannot be accurately captured by the classical Shannon capacity framework, since it relies on blocklengths that are practically infinite and therefore not suitable for short, latency-limited packets. Consequently, finite blocklength (FBL) information theory has emerged as a more accurate tool for evaluating the performance of short packet transmissions, providing tight approximations for decoding error probability in realistic IoT environments [4]–[7].

Massive IoT deployments are exposed to various security threats, with eavesdropping being one of the most fundamental. This issue becomes even more critical when IoT devices operate under energy, latency or hardware constraints, which often limits traditional cryptographic solutions. Physical layer security (PLS) provides a complementary approach by exploiting randomness in noise, fading and network geometry to ensure secure communications at the signal level. Although PLS has been extensively studied in large-scale wireless networks using stochastic geometry, most existing works rely on

the idealized infinite blocklength regime and therefore fail to capture the fundamental reliability and secrecy tradeoffs in short packet communications [8]–[10].

Despite the growing interest in both FBL communications and PLS, secure performance in massive IoT systems remains underexplored when all network entities, including potential adversaries, follow spatially random locations typically modeled through stochastic geometry. Although there are recent studies on PLS performance in the FBL regime [11]–[14], to the best of the authors’ knowledge, only a few existing works consider systems in which the eavesdropper is modeled as a spatially random node under a stochastic-geometry framework in the presence of FBL constraints [15], [16]. More importantly, to date there are no works analyzing PLS performance in the FBL regime for massive IoT networks in which both IoT nodes and base stations (BSs) follow spatial randomness.

Motivated by this research gap, this paper analyzes a massive IoT uplink network in which BSs and IoT devices are modeled as independent Poisson point processes (PPPs), while an eavesdropper is uniformly distributed within a disk of a certain radius around a transmitting IoT device. This model captures scenarios where an eavesdropper is located in the physical proximity of the targeted IoT device, representing local security threats common in massive IoT deployments. The analysis is conducted in the FBL regime, enabling accurate characterization of decoding error probabilities at both the intended BS and the eavesdropper. No prior work has examined the joint impact of stochastic interference, short-packet reliability, and the spatial uncertainty of the eavesdropper within a unified analytical framework. The analytical expressions for secure success probability, secrecy outage probability and secrecy throughput are derived and used to obtain numerical results in order to illustrate main system behavior under different system and channel parameters.

The rest of the paper is organized as follows. Section II introduces the system and channel model. Section III presents the FBL framework, while Section IV derives secrecy performance metrics under FBL. Section V provides numerical results and discussion, while Section VI concludes the paper.

## II. SYSTEM AND CHANNEL MODEL

### A. Network Geometry and Random Access Scheme

We consider an uplink massive IoT cellular network that connects a set of IoT devices deployed over  $\mathbb{R}^2$  plane, as depicted in Fig. 1. The IoT devices access the BSs using the

This article/publication is based upon work from COST Action 6G-PHYSEC (CA22168), supported by COST (European Cooperation in Science and Technology). This work has received funding from Serbian Ministry of Science, Technological Development and Innovation, through the Science and Technological Cooperation program Serbia-China, Research and development project No 00101957 2025 13440 003 000 620 021.

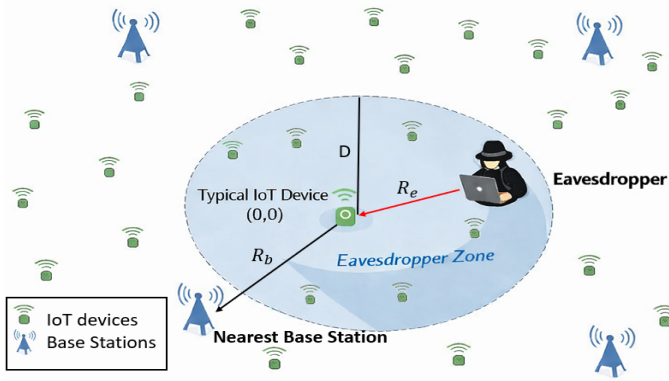


Fig. 1. System model.

slotted ALOHA protocol, with communication taking place in equal-length time slots. IoT devices are distributed according to a homogeneous PPP  $\Phi_u$  with density  $\lambda_u$  (devices/m<sup>2</sup>), while BSs are distributed according to an independent homogeneous PPP  $\Phi_b$  with density  $\lambda_b$  (BSs/m<sup>2</sup>). This spatial modeling approach is standard in the analysis of large-scale wireless networks and massive IoT systems [17], [18]. In each slot each device independently accesses the channel with probability  $p$ , resulting in an active PPP  $\Phi_a \subset \Phi_u$  with density  $\lambda_a = p\lambda_u$ . This baseline random-access massive IoT model follows [19]–[21]. To capture potential security threats, we also introduce a passive eavesdropper positioned at a random position around the typical IoT device, uniformly distributed within a disk of radius  $D$ , as presented in Fig. 1.

### B. Association and Distance Distributions

Each active IoT device associates with its geographically nearest BS. For a typical active device, let  $b_0 \in \Phi_b$  denote its serving BS, and let  $R_b$  be the corresponding distance. Under nearest-BS association in a PPP deployment (where the serving BS acts as Bob in the PLS framework), the probability density function (PDF) of  $R_b$  is given by [17]

$$f_{R_b}(r_b) = 2\pi\lambda_b r_b \exp(-\pi\lambda_b r_b^2), \quad r_b > 0, \quad (1)$$

which captures the well-known nearest-neighbor distribution in a homogeneous PPP.

### C. Eavesdropper Location Model

To incorporate the PLS aspect into considered massive IoT framework, we introduce a single passive eavesdropper (acting as Eve) whose goal is to intercept the uplink transmission of the typical active IoT device. The eavesdropper is positioned at a random location around the transmitting device, uniformly distributed within a disk of radius  $D$ . We denote by  $R_e$  the distance between the typical IoT device and the eavesdropper, whose PDF is

$$f_{R_e}(r_e) = \frac{2r_e}{D^2}, \quad 0 \leq r_e \leq D. \quad (2)$$

### D. Signal-to-Interference Ratio (SIR)

All IoT devices transmit with normalized unit power. Assuming an interference-limited regime, which is typical for uplink massive IoT networks, the instantaneous SIR at both the serving BS (Bob) and the eavesdropper (Eve) is defined as

$$\gamma_\star = \frac{G_\star H_\star R_\star^{-\eta}}{I_\star}, \quad (3)$$

where the subscript  $\star \in \{b, e\}$  is used as a generic index to distinguish between Bob and Eve.<sup>1</sup> The small-scale fading power gains of the channels toward the BS and the eavesdropper are denoted by  $H_b$  and  $H_e$ , respectively, while the corresponding aggregated interference terms are denoted by  $I_b$  and  $I_e$ . Large-scale path-loss is modeled as  $R_\star^{-\eta}$ , where  $\eta > 2$  is the path-loss exponent. The distances  $R_b$  and  $R_e$  are previously defined with the PDFs given by (1) and (2), respectively. In addition,  $G_b$  and  $G_e$  represent the receiver antenna gains at the BS and at the eavesdropper, respectively, which are not identical due to different hardware capabilities. The BS is equipped with sectorized or directional antennas that provide a higher receiver gain, while IoT-class devices employ compact omnidirectional antennas with limited gain.

### E. Small-Scale Fading Model

Small-scale fading is modeled by the Nakagami- $m$  distribution, thus the fading power gain follows a Gamma distribution with the PDF given as [22]

$$f_{H_\star}(h_\star) = \frac{m^m}{\Gamma(m)} h_\star^{m-1} e^{-mh_\star}, \quad h_\star > 0, \quad (4)$$

where  $\mathbb{E}[H_\star] = 1$ , and  $m \geq 1$  denotes the Nakagami- $m$  fading parameter. The same fading severity (i.e., identical parameter  $m$ ) is assumed for both the IoT–BS and IoT–eavesdropper links, while fading realizations remain independent across links. The Nakagami- $m$  model encompasses a wide range of fading conditions and is commonly adopted in massive IoT and cellular network analyses due to its analytical tractability.

### F. Interference Field and Statistics

All IoT devices are spatially distributed according to a homogeneous PPP  $\Phi_u \subset \mathbb{R}^2$ . Due to random access, only a fraction of devices are active at a given time, resulting in a thinned PPP of interferers. The aggregate uplink interference observed at receiver  $\star \in \{b, e\}$  is

$$I_\star = \sum_{i \in \Phi_u} a_i h_{i,\star} r_{i,\star}^{-\eta}, \quad (5)$$

where  $a_i \in \{0, 1\}$  denotes the activity indicator,  $h_{i,\star}$  is the fading coefficient,  $r_{i,\star}$  is the distance between the  $i$ -th interferer and receiver  $\star$  (being  $b$  for the legitimate receiver, i.e., the nearest BS, or  $e$  for the eavesdropper).

The distribution of the aggregate interference is characterized via its Laplace transform (LT). For PPP devices with

<sup>1</sup>Throughout the paper, the symbol  $\star \in \{b, e\}$  denotes either the legitimate receiver (Bob) or the eavesdropper (Eve).

slotted ALOHA access and Nakagami- $m$  fading, the LT of the interference power has the Kohlrausch–Williams–Watts (KWW) form [23]

$$\mathcal{L}_{I_*}(s) = \mathbb{E}[e^{-sI_*}] = \exp\left(-t s^{\frac{2}{\eta}}\right), \quad (6)$$

where

$$t = p\lambda_u\pi \frac{\Gamma\left(m + \frac{2}{\eta}\right)}{\Gamma(m) m^{\frac{2}{\eta}}} \Gamma\left(1 - \frac{2}{\eta}\right). \quad (7)$$

The same interference statistics apply at both the legitimate receiver and the eavesdropper, since interference is generated by the same PPP of active IoT devices.

The interference PDF can be obtained via inverse Laplace transform (ILT). In the special case  $\eta = 4$ , the interference follows a Lévy distribution [23]

$$f_{I_*}(x) = \frac{t \exp\left(-\frac{t_*^2}{4x}\right)}{2\sqrt{\pi} x^{3/2}}. \quad (8)$$

To perform the FBL analysis, we derive the conditional PDF of SIR  $\gamma_*$  defined in (3), conditioned on  $h_*$  and  $r_*$ . For  $\eta = 4$  and using the Lévy form of  $f_{I_*}$  in (8), the conditional PDF of SIR is obtained as

$$f_{\Gamma_*}(\gamma_* | h_*, r_*) = \frac{t \exp\left(-\frac{t_*^2 \gamma_*}{4G_* h_* r_*^4}\right)}{2\sqrt{\pi} G_* h_* r_*^4 \gamma_*}. \quad (9)$$

### III. FINITE BLOCKLENGTH DECODING MODEL

We consider short packet transmission, where codewords of length  $n$  channel uses are transmitted at a coding rate  $R$  bits per channel use. The block error probability conditioned on an instantaneous SIR, denoted by  $\gamma_*$  ( $\star \in \{b, e\}$ ), under FBL coding is well approximated by the normal approximation [4], [5]

$$\epsilon_{\star}(\gamma_{\star}) \approx Q\left(\sqrt{\frac{n}{V(\gamma_{\star})}}(C(\gamma_{\star}) - R)\right), \quad (10)$$

where  $C(\gamma_{\star}) = \log_2(1 + \gamma_{\star})$  is the Shannon capacity and  $V(\gamma_{\star}) = \gamma_{\star}(\gamma_{\star} + 2)(\log_2 e)^2 / (1 + \gamma_{\star})^2$  denotes the channel dispersion. Following the standard practice in stochastic-geometry-based FBL analysis, aggregate interference is treated as Gaussian noise [7], [19].

#### A. Block Error Probability at the Legitimate Receiver

Using the SIR  $\gamma_b$  at the serving BS (Bob), the unconditional uplink block error probability is determined as [21]

$$\begin{aligned} \epsilon_b &= \int_0^{\infty} \epsilon_b(\gamma_b) f_{\Gamma_b}(\gamma_b) d\gamma_b \\ &= \int_0^{\infty} \int_0^{\infty} \int_0^{\infty} \epsilon_b(\gamma_b) f_{\Gamma_b}(\gamma_b | h_b, r_b) f_{H_b}(h_b) f_{R_b}(r_b) d\gamma_b dh_b dr_b, \end{aligned} \quad (11)$$

where  $f_{R_b}(r_b)$ ,  $f_{H_b}(h_b)$  and  $f_{\Gamma_b}(\gamma_b | h_b, r_b)$  are the PDFs defined in (1), (4) and (9), respectively.

Since the integral in (11) can not be derived in a closed-form, we employ the linear approximation of the  $Q$ -function with the parameters  $\mu = \sqrt{\frac{n}{2\pi(2^{2R}-1)\log_2^2 e}}$ ,  $\theta = 2^R - 1$  and

$a = \sqrt{\frac{\pi}{2\mu^2}}$ . Following the derivation in [21], the uplink block error probability at the BS (Bob) is tightly approximated as

$$\begin{aligned} \epsilon_b &\approx \frac{a_1}{\Gamma(m)\pi} G_{3,3}^{2,3}\left(z_1 \left| \begin{matrix} 1, 0, \frac{1}{2} \\ \frac{1}{2}, m, 0 \end{matrix} \right. \right) - b_1 z_1 \left(c + dz_1^{m-\frac{1}{2}}\right) \\ &\quad + \frac{a_2}{\Gamma(m)\pi} G_{3,3}^{2,3}\left(z_2 \left| \begin{matrix} 1, 0, \frac{1}{2} \\ \frac{1}{2}, m, 0 \end{matrix} \right. \right) + b_2 z_2 \left(c + dz_2^{m-\frac{1}{2}}\right), \end{aligned} \quad (12)$$

where  $a_1 = \frac{1}{2} + \frac{\mu\theta}{\sqrt{2\pi}}$ ,  $a_2 = \frac{1}{2} - \frac{\mu\theta}{\sqrt{2\pi}}$ ,  $b_1 = \frac{\mu(\theta+a)}{\sqrt{2\pi}}$ ,  $b_2 = \frac{\mu(\theta-a)}{\sqrt{2\pi}}$ ,  $z_1 = \frac{t^2(\theta+a)m}{G_b(\lambda_b\pi)^2}$ ,  $z_2 = \frac{t^2(\theta-a)m}{G_b(\lambda_b\pi)^2}$ ,  $c = \frac{\Gamma(m-\frac{1}{2})}{3\sqrt{\pi}\Gamma(m)}$ ,  $d = \frac{(-1)^m m}{m+1}$ , and  $G_{\cdot, \cdot}^{a, \cdot}(\cdot | \cdot)$  is the Meijer G-function [24, (9.301)].

#### B. Block Error Probability at the Eavesdropper

The eavesdropper attempts to decode the same codeword at rate  $R$  under FBL constraints. Conditioned on the instantaneous SIR denoted by  $\gamma_e$  defined in (3), the block error probability under FBL at Eve is given by  $\epsilon_e(\gamma_e)$  in (10). Differently to the legitimate receiver, the eavesdropper location is uniformly distributed within a disk of radius  $D$  centered at the typical IoT device, resulting in a different SIR distribution.

Accordingly, the unconditional block error probability at the Eve is

$$\begin{aligned} \epsilon_e &= \int_0^{\infty} \epsilon_e(\gamma_e) f_{\Gamma_e}(\gamma_e) d\gamma_e \\ &= \int_0^D \int_0^{\infty} \int_0^{\infty} \epsilon_e(\gamma_e) f_{\Gamma_e}(\gamma_e | h_e, r_e) f_{H_e}(h_e) f_{R_e}(r_e) d\gamma_e dh_e dr_e, \end{aligned} \quad (13)$$

where  $f_{R_e}(r_e)$ ,  $f_{H_e}(h_e)$  and  $f_{\Gamma_e}(\gamma_e | h_e, r_e)$  are the PDFs defined in (2), (4) and (9), respectively.

Using the same linear approximation of the  $Q$ -function as for Bob [21], after following derivation summarized in Appendix A, the block error probability at Eve is tightly approximated as

$$\begin{aligned} \epsilon_e &\approx B \left( G_{5,7}^{2,5}\left(y_1 \left| \begin{matrix} -\frac{1}{4}, 0, \frac{1}{4}, \frac{1}{2}, 1 \\ \frac{1}{2}, m, 0, -\frac{1}{2}, -\frac{1}{4}, 0, \frac{1}{4} \end{matrix} \right. \right) \right. \\ &\quad \left. + A G_{5,7}^{2,5}\left(y_2 \left| \begin{matrix} -\frac{1}{4}, 0, \frac{1}{4}, \frac{1}{2}, 1 \\ \frac{1}{2}, m, 0, -\frac{1}{2}, -\frac{1}{4}, 0, \frac{1}{4} \end{matrix} \right. \right) \right) \\ &\quad + C_2 G_{5,7}^{2,5}\left(y_2 \left| \begin{matrix} -\frac{3}{4}, -\frac{1}{2}, -\frac{1}{4}, 0, -\frac{1}{2} \\ -\frac{3}{2}, 0, m-\frac{1}{2}, -1, -\frac{3}{4}, -\frac{1}{2}, -\frac{1}{4} \end{matrix} \right. \right) \\ &\quad - C_1 G_{5,7}^{2,5}\left(y_1 \left| \begin{matrix} -\frac{3}{4}, -\frac{1}{2}, -\frac{1}{4}, 0, -\frac{1}{2} \\ -\frac{3}{2}, 0, m-\frac{1}{2}, -1, -\frac{3}{4}, -\frac{1}{2}, -\frac{1}{4} \end{matrix} \right. \right), \end{aligned} \quad (14)$$

where  $y_1 = \frac{D^4 t^2 (\theta+a)m}{4G_e}$ ,  $y_2 = \frac{D^4 t^2 (\theta-a)m}{4G_e}$ ,  $A = \frac{1}{2} - \frac{\mu\theta}{\sqrt{2\pi}}$ ,  $B = \frac{2D}{\eta\sqrt{\pi}\Gamma(m)}$ ,  $C_1 = \frac{D^3 t \mu \sqrt{m} (\theta+a)^{\frac{3}{2}}}{\sqrt{2\pi}\Gamma(m)\eta}$ ,  $C_2 = \frac{D^3 t \mu \sqrt{m} (\theta-a)^{\frac{3}{2}}}{\sqrt{2\pi}\Gamma(m)\eta}$ .

### IV. SECRECY METRICS UNDER FINITE BLOCKLENGTH

In short-packet massive IoT systems, secrecy is inherently linked to the decoding outcomes at both the legitimate receiver and the eavesdropper. Unlike classical information-theoretic secrecy metrics based on asymptotic capacity, FBL communication exhibits a smooth transition between successful and unsuccessful decoding. Motivated by this observation, we adopt a decoding-based secrecy formulation, which has recently emerged as a meaningful operational security metric for short-packet wireless systems [25].

### A. Finite Blocklength Secure Success Probability

A transmission is said to be securely successful if the legitimate BS Bob decodes the packet correctly, while the eavesdropper Eve fails to decode it, i.e., the secure success event is defined as

$$\mathcal{S} \triangleq \{\text{Bob decodes}\} \cap \{\text{Eve fails}\}. \quad (15)$$

Decoding outcomes at Bob and Eve are assumed to be independent. Therefore, the conditional secure success probability is determined as

$$\mathbb{P}(\mathcal{S} | \gamma_b, \gamma_e) = (1 - \epsilon_b(\gamma_b))\epsilon_e(\gamma_e). \quad (16)$$

Averaging over the SIRs  $\gamma_e$  and  $\gamma_b$ , i.e., over the spatial randomness, fading, and random access activity, yields the secure success probability

$$P_{\text{sec}} \triangleq \mathbb{P}(\mathcal{S}) = (1 - \epsilon_b)\epsilon_e, \quad (17)$$

where  $\epsilon_b$  and  $\epsilon_e$  are previously derived in (12) and (14), respectively.

This metric captures the joint impact of interference, network geometry, and FBL decoding on security performance. Unlike the conventional secrecy outage probability, which is defined based on Shannon secrecy capacity in the infinite blocklength regime,  $P_{\text{sec}}$  captures decoding outcomes under FBL transmission, providing an operational measure of secrecy in short-packet communications.

### B. Finite Blocklength Secrecy Outage Probability

The FBL secrecy outage probability is defined as the probability that secure success does not occur, i.e.,

$$P_{\text{out}} \triangleq 1 - P_{\text{sec}} = 1 - (1 - \epsilon_b)\epsilon_e. \quad (18)$$

This definition reflects an operational notion of secrecy that is well suited to short packet transmission and contrasts with classical secrecy outage formulations based solely on Shannon secrecy capacity [26], [27].

### C. Secrecy Throughput

To jointly account for random access, FBL reliability, and secrecy, we define the per-device secrecy throughput (bits/channel-use) as

$$T_{\text{sec}} \triangleq p R P_{\text{sec}} = p R (1 - \epsilon_b)\epsilon_e. \quad (19)$$

This definition is consistent with throughput formulations in massive IoT networks, while explicitly incorporating secrecy constraints [21], [27].

## V. NUMERICAL RESULTS

In this section, we present numerical results to evaluate the FBL secrecy performance of the considered uplink massive IoT network. Unless otherwise stated, a baseline configuration assumes a BS with  $G_b = 15$  dBi (i.e.,  $G_b = 31.6$ ) and an IoT-class eavesdropper with  $G_e = 0$  dBi (i.e.,  $G_e = 1$ ).

Fig. 2 shows the secure success probability  $P_{\text{sec}}$  as a function of the IoT device density  $\lambda_u$  for different coding rates  $R$  and eavesdropper radius  $D$ . As the IoT density increases,

the secure success probability improves for all considered parameter settings. This behavior is due to the increased aggregate interference at the eavesdropper, which degrades its decoding capability more severely than that of the legitimate receiver. Larger values of the eavesdropper radius  $D$  further enhance secrecy performance, since a wider region for the eavesdropper's placement increases the likelihood that it is located farther from the IoT device, resulting in a lower received signal power at Eve. For a fixed eavesdropper radius, lower coding rates yield higher values of  $P_{\text{sec}}$ , reflecting the improved decoding reliability at the legitimate receiver under FBL transmission. In particular, when  $D = 100$  m, the secure success probability approaches unity even at moderate IoT densities, indicating that the spatial separation of eavesdropper plays a dominant role in enhancing physical layer security in dense IoT networks, further highlighting that sufficiently large eavesdropper regions significantly mitigate interception capabilities.

Fig. 3 shows the secrecy outage probability  $P_{\text{out}}$  as a function of the BS antenna gain  $G_b$  for different BS densities  $\lambda_b$  and access probabilities  $p$ . It is observed that  $P_{\text{out}}$  decreases monotonically as  $G_b$  increases for all considered network parameters. This behavior is due to the improved received signal strength at the BS with increasing antenna gain, which enhances the decoding reliability of the legitimate receiver. For a fixed  $G_b$ , a higher BS density results in a lower outage probability, as the effects of uplink interference are mitigated. Moreover, the curves corresponding to a smaller access probability  $p = 10^{-2}$  exhibit lower outage levels compared to those with  $p = 5 \times 10^{-2}$ , since reduced channel access alleviates aggregate interference. The performance gap among different values of  $\lambda_b$  and  $p$  becomes more pronounced at higher antenna gains, highlighting the dominant role of interference in determining secrecy outage performance.

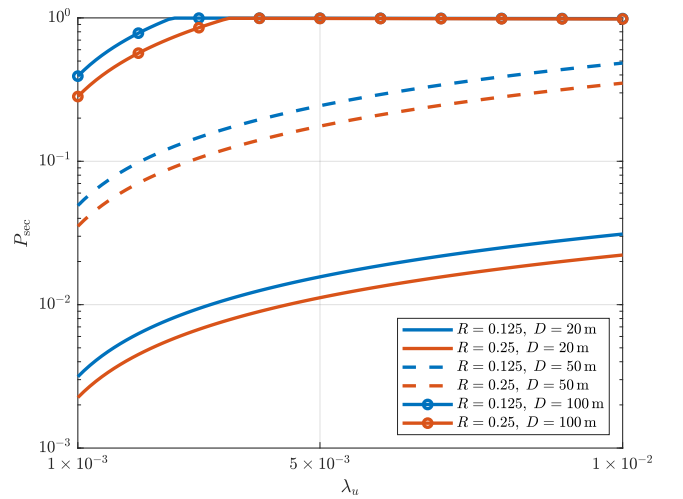


Fig. 2.  $P_{\text{sec}}$  versus the IoT device density  $\lambda_u$  for coding rates  $R \in \{1/8, 1/4\}$ , distances  $D \in \{20 \text{ m}, 50 \text{ m}, 100 \text{ m}\}$ , with a fixed blocklength  $n = 128$  and Nakagami parameter  $m = 1$ . BS density is  $\lambda_b = 10^{-4}$ , with activation probability  $p = 0.001$ .

## VI. CONCLUSION

This paper presented a PLS analysis of massive uplink IoT networks operating under FBL constraints. By incorporating stochastic interference, Nakagami- $m$  fading and the spatial uncertainty of an eavesdropper, analytical expressions for key secrecy metrics, including the secure success probability, secrecy outage probability and secrecy throughput, have been derived. Numerical results illustrate a strong dependence of secure performance on network density and the relative proximity of the eavesdropper. These results confirm the validity of the analytical framework and provide useful insights for the design of secure short packet communication in dense IoT deployments. Future work may extend the framework to multi-eavesdropper scenarios or systems with adaptive transmission strategies.

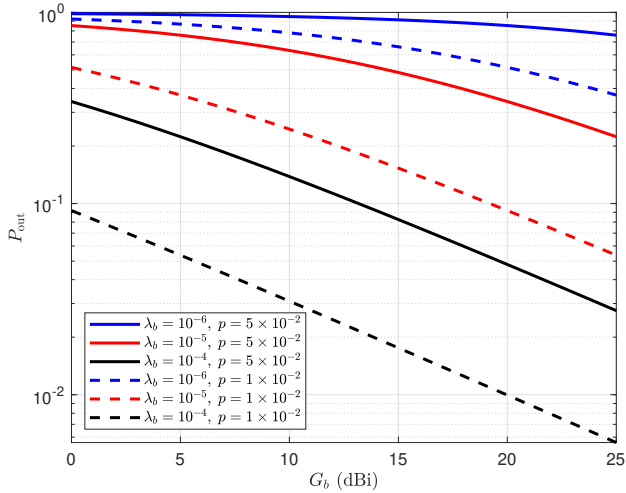


Fig. 3.  $P_{\text{out}}$  as a function of the BS antenna gain  $G_b$  for three BS densities,  $\lambda_b \in \{10^{-6}, 10^{-5}, 10^{-4}\}$ , and two access probabilities,  $p = 5 \times 10^{-2}$  and  $p = 10^{-2}$ . The coding rate is  $R = 1/4$ , distance  $D = 100$  m, user density  $\lambda_u = 10^{-3}$ , blocklength  $n = 128$ , and Nakagami parameter  $m = 4$ .

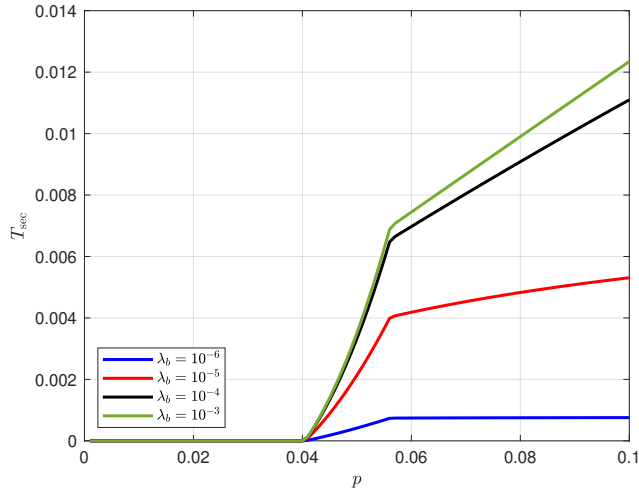


Fig. 4.  $T_{\text{sec}}$  as a function of the access probability  $p$ , blocklength  $n = 512$ , and four BS densities,  $\lambda_b \in \{10^{-6}, 10^{-5}, 10^{-4}, 10^{-3}\}$ , rate  $R = 1/8$ , distance  $D = 150$  m, user density  $\lambda_u = 10^{-3}$  and parameter  $m = 2$ .

Fig. 4 depicts the secure throughput  $T_{\text{sec}}$  derived in (19) as a function of the access probability  $p$  for different BS densities. As  $p$  increases, the secure throughput initially remains close to zero and then increases monotonically once reliable decoding at the BS becomes feasible. This threshold behavior is a consequence of FBL transmission, where the decoding error probability at the legitimate receiver remains close to one (e.g.,  $P_{\text{sec}}$  and  $T_{\text{sec}}$  close to zero) until the effective SIR exceeds a minimum level. For a fixed access probability, higher BS density improve the secure throughput by reducing the decoding error probability at the base station. These results highlight the importance of access control and network densification in maximizing secure throughput in massive IoT networks under FBL constraints.

## APPENDIX A

Based on linear approximation of the Q-function [21], (13) and the parameters  $\mu$ ,  $\theta$  and  $a$  are defined in Section III.B, the error probability of the eavesdropper can be approximated as

$$\begin{aligned} \epsilon_e &\approx \int_0^D \int_0^\infty \int_0^{\theta-a} f_{\Gamma_e}(\gamma_e | h_e, r_e) f_{H_e}(h_e) f_{R_e}(r_e) d\gamma_e dh_e dr_e \\ &+ \int_0^D \int_0^\infty \int_{\theta-a}^{\theta+a} \left( \frac{1}{2} - \frac{\mu(\gamma_e - \theta)}{\sqrt{2\pi}} \right) \\ &\times f_{\Gamma_e}(\gamma_e | h_e, r_e) f_{H_e}(h_e) f_{R_e}(r_e) d\gamma_e dh_e dr_e \\ &= I_1 + I_2 - I_3 + I_4, \end{aligned} \quad (20)$$

where the triple integrals in (20) are defined as follows

$$I_1 = \int_0^D \int_0^\infty \int_0^{\theta-a} f_{\Gamma_e}(\gamma_e | h_e, r_e) f_{H_e}(h_e) f_{R_e}(r_e) d\gamma_e dh_e dr_e, \quad (21)$$

$$I_2 = \frac{1}{2} \int_0^D \int_0^\infty \int_{\theta-a}^{\theta+a} f_{\Gamma_e}(\gamma_e | h_e, r_e) f_{H_e}(h_e) f_{R_e}(r_e) d\gamma_e dh_e dr_e, \quad (22)$$

$$I_3 = \frac{\mu}{\sqrt{2\pi}} \int_0^D \int_0^\infty \int_{\theta-a}^{\theta+a} \gamma_e f_{\Gamma_e}(\gamma_e | h_e, r_e) f_{H_e}(h_e) f_{R_e}(r_e) d\gamma_e dh_e dr_e, \quad (23)$$

$$I_4 = \frac{\mu\theta}{\sqrt{2\pi}} \int_0^D \int_0^\infty \int_{\theta-a}^{\theta+a} f_{\Gamma_e}(\gamma_e | h_e, r_e) f_{H_e}(h_e) f_{R_e}(r_e) d\gamma_e dh_e dr_e, \quad (24)$$

where  $f_{R_e}(r_e)$ ,  $f_{H_e}(h_e)$  and  $f_{\Gamma_e}(\gamma_e | h_e, r_e)$  are the PDFs defined in (2), (4) and (9), respectively.

The integrals  $I_1$ ,  $I_2$  and  $I_4$  have a similar form. After substituting (2), (4) and (9) into (21), i.e., (22) or (24), the following rules are applied: [24, (8.251)], [28, (01.03.26.0004.01), (06.25.26.0006.01), (07.34.21.0011.01), (07.34.21.0011.01) and (07.34.21.0084.01)]. The integrals  $I_1$ ,  $I_2$  and  $I_4$  are derived as

$$I_1 = \frac{2D}{\Gamma(m)\sqrt{\pi\eta}} G_{5,7}^{2,5} \left( \frac{D^4 t^2 (\theta - a) m}{4G_e} \middle| \begin{matrix} -\frac{1}{4}, 0, \frac{1}{4}, \frac{1}{2}, 1 \\ \frac{1}{2}, m, 0, -\frac{1}{2}, -\frac{1}{4}, 0, \frac{1}{4} \end{matrix} \right), \quad (25)$$

$$I_2 = \frac{D}{\sqrt{\pi}\Gamma(m)\eta} \left( G_{5,7}^{2,5} \left( \frac{D^4 t^2 (\theta + a) m}{4G_e} \middle| \begin{matrix} -\frac{1}{4}, 0, \frac{1}{4}, \frac{1}{2}, 1 \\ \frac{1}{2}, m, 0, -\frac{1}{2}, -\frac{1}{4}, 0, \frac{1}{4} \end{matrix} \right) - G_{5,7}^{2,5} \left( \frac{D^4 t^2 (\theta - a) m}{4G_e} \middle| \begin{matrix} -\frac{1}{4}, 0, \frac{1}{4}, \frac{1}{2}, 1 \\ \frac{1}{2}, m, 0, -\frac{1}{2}, -\frac{1}{4}, 0, \frac{1}{4} \end{matrix} \right) \right), \quad (26)$$

$$I_4 = \frac{2\mu\theta}{\Gamma(m)\pi\sqrt{2}\eta} \left( G_{5,7}^{2,5} \left( \frac{D^4 t^2 (\theta + a) m}{4G_e} \middle| \begin{matrix} -\frac{1}{4}, 0, \frac{1}{4}, \frac{1}{2}, 1 \\ \frac{1}{2}, m, 0, -\frac{1}{2}, -\frac{1}{4}, 0, \frac{1}{4} \end{matrix} \right) - G_{5,7}^{2,5} \left( \frac{D^4 t^2 (\theta - a) m}{4G_e} \middle| \begin{matrix} -\frac{1}{4}, 0, \frac{1}{4}, \frac{1}{2}, 1 \\ \frac{1}{2}, m, 0, -\frac{1}{2}, -\frac{1}{4}, 0, \frac{1}{4} \end{matrix} \right) \right). \quad (27)$$

After substituting (2), (4) and (9) into (23), and applying the rules [28, (01.03.26.0004.01), (06.34.26.0005.01), (07.34.16.0002.01)(07.34.21.0011.01), (07.34.16.0002.01), and (07.34.21.0084.01)], the integral  $I_3$  is derived as

$$I_3 = C_2 G_{5,7}^{2,5} \left( y_2 \middle| \begin{matrix} -\frac{3}{4}, -\frac{1}{2}, -\frac{1}{4}, 0, -\frac{1}{2} \\ -\frac{3}{2}, 0, m - \frac{1}{2}, -1, -\frac{3}{4}, -\frac{1}{2}, -\frac{1}{4} \end{matrix} \right) - C_1 G_{5,7}^{2,5} \left( y_1 \middle| \begin{matrix} -\frac{3}{4}, -\frac{1}{2}, -\frac{1}{4}, 0, -\frac{1}{2} \\ -\frac{3}{2}, 0, m - \frac{1}{2}, -1, -\frac{3}{4}, -\frac{1}{2}, -\frac{1}{4} \end{matrix} \right), \quad (28)$$

where  $y_1$ ,  $y_2$ ,  $C_1$  and  $C_2$  are defined in Section III.B. After substituting (25), (26), (27) and (28) into (20), final approximate FBL error probability is derived and given by (14).

#### REFERENCES

- [1] M. Shafi et al., "5G: A Tutorial Overview of Standards, Trials, Challenges, Deployment, and Practice," *IEEE J. Sel. Areas Commun.*, vol. 35, no. 6, pp. 1201-1221, 2017.
- [2] M. Shirvanimoghaddam, M. Dohler, and S. J. Johnson, "Massive Non-Orthogonal Multiple Access for Cellular IoT: Potentials and Limitations," *IEEE Commun. Mag.*, vol. 55, no. 9, pp. 55-61, 2017.
- [3] U. Raza, P. Kulkarni, and M. Sooriyabandara, "Low power wide area networks: An overview," *IEEE Commun. Surveys Tuts.*, vol. 19, no. 2, pp. 855-873, 2017.
- [4] Y. Polyanskiy, H. V. Poor, and S. Verdú, "Channel coding rate in the finite blocklength regime," *IEEE Trans. Inf. Theory*, vol. 56, no. 5, pp. 2307-2359, 2010.
- [5] G. Durisi, T. Koch, and P. Popovski, "Toward massive, ultrareliable, and low-latency wireless communication with short packets," *Proc. IEEE*, vol. 104, no. 9, pp. 1711-1726, 2016.
- [6] G. Durisi, T. Koch, J. Östman, Y. Polyanskiy, and W. Yang, "Short-packet communications over multiple-antenna Rayleigh-fading channels," *IEEE Trans. Commun.*, vol. 64, no. 2, pp. 618-629, 2016.
- [7] B. Makki, T. Svensson, and M. Zorzi, "Finite block-length analysis of spectrum sharing networks: Interference-constrained scenario," *IEEE Wireless Commun. Lett.*, vol. 4, no. 4, pp. 433-436, 2015.
- [8] H. Wang, X. Zhou, and M. C. Reed, "Physical Layer Security in Cellular Networks: A Stochastic Geometry Approach," *IEEE Trans. Wireless Commun.*, vol. 12, no. 6, pp. 2776-2787, 2013.
- [9] T.-X. Zheng, X. Chen, C. Wang, K. -K. Wong, and J. Yuan, "Physical Layer Security in Large-Scale Random Multiple Access Wireless Sensor Networks: A Stochastic Geometry Approach," *IEEE Trans. Wireless Commun.*, vol. 70, no. 6, pp. 4038-4051, 2022.
- [10] H. Chamkhia, A. Erbad, A. Mohamed, A. R. Hussein, A. K. Al-Ali, and M. Guizani, "Stochastic Geometry-Based Physical-Layer Security Performance Analysis of a Hybrid NOMA-PDM-Based IoT System," *IEEE Internet of Things J.*, vol. 11, no. 2, pp. 2027-2042, 2024.
- [11] C. Feng, H.-M. Wang, and H. V. Poor, "Reliable and Secure Short-Packet Communications," *IEEE Trans. Wireless Commun.*, vol. 21, no. 3, pp. 1913-1926, 2022.
- [12] M. Tatar Mamaghani, X. Zhou, N. Yang, A. Lee Swindlehurst, and H. V. Poor, "Performance Analysis of Finite Blocklength Transmissions Over Wiretap Fading Channels: An Average Information Leakage Perspective," *IEEE Trans. Wireless Commun.*, vol. 23, no. 10, pp. 13252-13266, 2024.
- [13] T.-X. Zheng, H.-M. Wang, D. W. K. Ng, and J. Yuan, "Physical-Layer Security in the Finite Blocklength Regime Over Fading Channels," *IEEE Trans. Wireless Commun.*, vol. 19, no. 5, pp. 3405-3420, 2020.
- [14] A. Vázquez-Castro and M. Hayashi, "Physical Layer Security for RF Satellite Channels in the Finite-Length Regime," *IEEE Trans. Inf. Forensics Secur.*, vol. 14, no. 4, pp. 981-993, 2019.
- [15] J. Farhat, G. Brante, R. D. Souza, and J. P. Vilela, "On the Secure Spectral Efficiency of URLLC With Randomly Located Colluding Eavesdroppers," *IEEE Internet of Things J.*, vol. 8, no. 19, pp. 14672-14682, 2021.
- [16] R. Ma, W. Yang, L. Tao, X. Lu, Z. Xiang, and J. Liu, "Covert Communications With Randomly Distributed Wardens in the Finite Blocklength Regime," *IEEE Trans. Veh. Technol.*, vol. 71, no. 1, pp. 533-544, 2022.
- [17] M. Haenggi, *Stochastic Geometry for Wireless Networks*. Cambridge Univ. Press, 2012.
- [18] T. D. Novlan, H. S. Dhillon, and J. G. Andrews, "Analytical modeling of uplink cellular networks," *IEEE Trans. Wireless Commun.*, vol. 12, no. 6, pp. 2669-2679, 2013.
- [19] N. Hesham and A. Chaaban, "On the performance of large-scale wireless networks in the finite blocklength regime," *Proc. IEEE ICC*, 2021.
- [20] N. Hesham, J. Hossain, and A. Chaaban, "Transmission rate analysis for large-scale uplink networks in the finite blocklength regime," *Proc. IEEE WCNC*, 2023.
- [21] T. Devaja, M. Petkovic, C. Wang, M. Beko, and D. Vukobratovic, "On error probability analysis of short-packet communications in massive Internet of Things," *IEEE Access*, vol. 12, pp. 67107-67116, 2024.
- [22] M. K. Simon, M.-S. Alouni, *Digital communication over fading channels*, 2nd ed. New York, Wiley, 2004.
- [23] H. A. Ammar, Y. Nasser, and H. Artail, "Closed-form expressions for the probability density function of the interference power in PPP networks," *Proc. IEEE ICC*, 2018.
- [24] I. Gradshteyn and I. Ryzhik, *Table of Integrals, Series, and Products*, 5th ed., Academic Press, 1994.
- [25] A. Mukherjee et al., "Principles of physical layer security in multiuser wireless networks: A survey," *IEEE Commun. Surveys Tuts.*, vol. 16, no. 3, pp. 1550-1573, 2014.
- [26] P. K. Gopala, L. Lai, and H. El Gamal, "On the secrecy capacity of fading channels," *IEEE Trans. Inf. Theory*, vol. 54, no. 10, pp. 4687-4698, 2008.
- [27] X. Zhou, R. K. Ganti, J. G. Andrews, and A. Hjørungnes, "On the throughput cost of physical layer security in decentralized wireless networks," *IEEE Trans. Wireless Commun.*, vol. 10, no. 8, pp. 2764-2775, 2011.
- [28] *The Wolfarm Functions Site*. [Online]. Available: <http://functions.wolfarm.com>